




Efficiency enhancement and chrono-photoelectron generation in dye-sensitized solar cells based on spin-coated TiO₂ nanoparticle multilayer photoanodes and a ternary iodide gel polymer electrolyte

T. M. W. J. Bandara¹, S. M. S. Gunathilake¹, G. B. M. M. M. Nishshanke¹, M. A. K. L. Dissanayake², N. B. Chaure³, O. I. Olusola⁴, B.-E. Mellander⁵, M. Furlani⁶, and Ingvar Albinsson^{6,*} 

¹ Department of Physics and Postgraduate Institute of Science, University of Peradeniya, Peradeniya, Sri Lanka

² National Institute of Fundamental Studies, Hantana Road, Kandy, Sri Lanka

³ Department of Physics, Savitribai Phule Pune University, Pune-7, India

⁴ Department of Physics, The Federal University of Technology Akure, Akure, Nigeria

⁵ Department of Physics, Chalmers University of Technology, Gothenburg, Sweden

⁶ Department of Physics, University of Gothenburg, 41296 Gothenburg, Sweden

Received: 1 June 2023

Accepted: 2 September 2023

© The Author(s), 2023

ABSTRACT

The effect of the thickness of a multilayer TiO₂ photoanode on the performance of a dye-sensitized solar cell (DSC) made with a polyethylene oxide-based gel polymer electrolyte containing ternary iodides and performance enhancer 4-tert-butylpyridine is studied. Multilayer photoanodes consisting of up to seven layers of TiO₂ nano-particles (13 nm and 21 nm) are prepared by spin coating of successive layers. XRD results confirm the predominant presence of the anatase phase of TiO₂ in the multilayer structure after sintering. The SEM images reveal the formation of a single TiO₂ film upon sintering due to merging of individually deposited layers. The photocurrent density (J_{SC}) and the efficiency increase with the number of TiO₂ layers exhibiting the maximum efficiency and J_{SC} of 5.5% and 12.5 mA cm⁻², respectively, for the 5-layered electrode of total thickness 4.0 μm with a 9.66×10^{-8} mol cm⁻² surface dye concentration. The present study introduces a method of determining the rate of effective photoelectron generation and the average time gap between two successive photon absorptions where the respective results are 1.34 molecule⁻¹ s⁻¹ and 0.74 s for the most efficient cell studied in this work.

Address correspondence to E-mail: ingvar.albinsson@gu.se

1 Introduction

Dye-sensitized solar cells (DSCs) are a favorable alternative to conventional photovoltaic (PV) technologies due to their easy fabrication and cost effectiveness [1–3]. The active photoelectrode of a DSC is, in general, a dye-sensitized mesoporous oxide thin film, while the typical counter-electrodes consist of a thin electro-catalytic layer of platinum or carbon [4, 5]. The electrolyte in a DSC assembly usually comprises an organic solvent containing a redox mediator, which is sandwiched between the photoelectrode and the counter-electrode. The most critical component is the photoelectrode that harvests light energy, which needs more research on structural and morphological modifications in order to optimize the loading and homogeneous distribution of the dye without degrading the electrical conductivity. In this study, we have focused our attention on improving the efficiency and stability of DSC by optimizing the light-harvesting ability of the multi-layered TiO₂ photoanode using a highly reproducible fabrication method and a gel polymer electrolyte that contains a ternary mixture of iodides with the intention of improving the efficiency and stability of the DSCs.

High-performing TiO₂ films are essential not only to be used as a membrane for DSCs, but also important to making membranes for self-cleaning [6, 7], lithium-ion batteries [8, 9], and photocatalysts [10, 11]. Thus, the TiO₂ multilayer electrode investigated in this study can be utilized not only in DSCs, but also in numerous other applications.

1.1 Semiconductor photoanode

The structure, morphology, and type of wide band-gap semiconductor used in the photoanode of a DSC play a crucial role since the light-harvesting species (dye molecules) are adsorbed onto its surface. Further, the semiconductor films collect the excited electrons from the photosensitizer, which need to be transported to the current collector and finally to the counter-electrode through the external load [12, 13]. Although a wide range of metal oxides, such as ZnO, SnO₂, Nb₂O₅, and TiO₂, are utilized as the semiconductor material in photoanodes, TiO₂ offers more advantages due to its non-toxicity, high abundance, greater stability, and ease of preparing mesoporous thin films [4, 14]. TiO₂ has three crystalline phases, namely rutile, anatase, and brookite [15]. Among these forms, mesoporous

anatase is the most preferred thin film structure for DSC applications due to its befitting optical and electrical properties, such as the band gap (3.2 eV), and band edge energy as well as the electrical properties such as high mobility and number density of carriers, which finally lead to produce prominent photocurrents and photovoltages [14, 16, 17].

In 1991, O'Regan and Grätzel achieved an overall energy conversion efficiency of around 7% by fabricating a DSC using a 10- μ m-thick nano-structured thin film of a few nanometer-sized TiO₂ particles [1]. A variety of one-dimensional morphological structures of TiO₂, such as nanofibers [18, 19], nanowires [20–22], nano-rods [23], and nanotubes [24], which offer high surface-to-volume ratios, are utilized in the photoanode to enhance the efficiency of DSCs. Further, monolayer [31], double-layer [25, 26], or triple-layer [27, 28] TiO₂ nano-structured thin films have intensively been studied. For instance, Wang et al. have achieved a DSC efficiency of 8.03% and a short-circuit current density of 15.7 mA cm⁻² by utilizing electro-spun multi-layered composite photoanodes composed of TiO₂ nano-particles and nano-rods [29].

Increasing the surface roughness of the semiconductor film is a promising method to boost the efficiency of a DSC, since high surface roughness increases the specific surface area and improves the light harvesting by enhancing the surface density of adsorbed dye molecules [1]. Therefore, an efficient photoanode should possess a high specific surface area as well as a favorable surface morphology in order to maximize the light scattering and absorption ability [30]. Therefore, recently, photoanodes having nanoparticle multi-layered architectures have been readily investigated due to their excellent dye loading ability and light-scattering capability, plus other advantages such as the controllable layer thickness [31–35].

There are various TiO₂ thin film preparation methods, such as doctor blade [36, 37], screen printing [38, 39], dip coating, electro-spinning, and spin coating [40, 41]. The spin coating is a highly reproducible and low-cost method for preparing metal oxide photoanodes. The rotation speed and the composition of the colloidal suspension are the main parameters that govern the properties of spin-coated films [42, 43]. For other widely used TiO₂ film deposition methods such as doctor blade, screen printing, and dip coating, the film quality depends on many parameters including the total solids in suspension, suspension volume, blade speed, blade pressure, and blade land

length [44, 45]. In addition, the spin coating technique provides a fissile way of preparing homogeneous multi-layered structures with controllable thickness and morphology.

Current–voltage (I – V) characterization is the conventional way of measuring the performance of solar cells. The cell performance dependence on potential scan rate [46, 47], irradiance [25, 48], illumination time [49], and surface adsorbed dye concentration [50, 51] demands at least to give the potential scan rate, irradiance, the time dependence of the cell permeance at least for a short period, and the surface dye concentration of the photoelectrode, respectively. According to a recent report, a quasi-solid state solar cell fabricated by combining a photoanode consisting of four layers of TiO_2 nano-particles of average particle size of ~ 21 nm along with a polyacrylonitrile-based electrolyte that contains binary salts of RbI and tetrahexylammonium iodide (Hex_4NI) exhibited an efficiency of 7.5% and short-circuit current density (J_{SC}) of 20.0 mA cm^{-2} at 1000 W m^{-2} irradiance under a 10 mV s^{-1} scan rate [52]. However, the optimization of the film thickness and the number of layers that govern the dye loading is very important for DSC research. Therefore, in the present study, two different particle sizes (13 nm and 21 nm) were used to prepare multilayer TiO_2 photoanodes. In the present investigation, crack-free multi-layered photoanodes composed of 1, 2, 3, ..., 7 successive layers were successfully coated on fluorine-doped tin-oxide (FTO) substrates, using a wet chemical method. Finally, a series of quasi-solid-state DSCs was fabricated by employing multi-layered photoanodes consisting of 1–7 layers of spin-coated TiO_2 nano-particles of the size 13 nm and 21 nm. The present study introduces a new method to find the rate of effective photoelectron generation and the average time gap between two successive photon absorptions by dye molecules, combining dye absorption calculations and the photoelectrical performance of DSSCs. The method and calculation would be helpful to determine photoelectron generation and, thus, optimize photocurrents since similar methods or calculations are not found in the literature.

1.2 Gel polymer electrolyte

In a DSC, the electrolyte governs the electron transfer kinetics at the photoanode and counter-electrode interfaces as well as the ion transport dynamics in the bulk [2, 53]. The electrolyte should be a good ionic

conductor to achieve an efficient and steady charge transfer at two interfaces [54]. In general, liquid electrolytes provide higher conductivity and interfacial charge transfer. However, in recent times, quasi-solid-state electrolytes have gained a greater attention than liquid electrolytes for the fabrication of DSCs since they can overcome most of the shortcomings present in liquid electrolytes, such as the poor long-term stability caused by leakage and volatilization of liquids and desorption as well as degradation of the dye [55–57].

There are some recent advancements in the use of solid or gel polymer electrolytes in DSCs which offer chemical and physical stability along with considerably higher efficiencies. In particular, the use of composite polymer electrolytes based on 1-d nanofiber fillers and reduced graphene oxide are novel approaches [58, 59]. In addition, for the efficient charge collection and charge separation process, patterning the photoanode and the use of a metal grid are some of the practical approaches used to improve the performance of DSCs [60, 61]. The super-hydrophobic polymeric architecture introduced by Bella et al. realized the method to make floating third-generation solar cells [62]. In addition, novel ways to improve gel polymer electrolytes for DSCs are reported. For instance, DSCs with gel polymers that contain water have certain advantages and recorded higher stability along with considerable efficiency [63, 64].

In this study, we have avoided the use of volatile solvents such as acetonitrile, to the DSC electrolyte but used controlled amounts of nonvolatile solvents, ethylene carbonate (EC) and propylene carbonate (PC) to jellify the electrolyte and to improve ionic conductivity and the stability of the cells.

In the recent past, several efforts have been made to improve the ionic conductivity of gel polymer electrolytes based on various polymers such as polyethylene oxide (PEO), poly(acrylonitrile), poly(vinyl chloride), poly(vinyl pyrrolidinone), poly(vinylidene ester), poly(methyl methacrylate), and poly(vinylidene fluoride), intended to be utilized in DSCs [2, 55, 65]. Moreover, it has been confirmed that the incorporation of binary and ternary iodide salt systems, having cations with high and low charge densities (charge to volume ratio) into gel polymer electrolytes, is a reliable technique to enhance the efficiency of a DSC [66–68].

The incorporation of the additives like 1-methyl-3-propylimidazolium iodide (MPII) [69] and 4-tert-butylpyridine (4TBP) [70, 71] to the electrolyte

system also contributes to improve the performance of DSCs. In the previous studies, the effects of additives/performance enhancers, such as MPPII and 4TBP, on the function of quasi-solid-state DSCs were explained in detail [72]. The compositions MPPII of (4TBP) [71, 72] and binary salts [73] optimized in previous studies were used in this work in the polymer electrolyte gel to obtain high-performance DSCs. In order to harness, the synergistic benefits of the improved photoanode, and improved polymer electrolyte, seven DSCs were investigated in detail in this work by incorporating TiO₂ multilayered photoanodes and a PEO-based gel polymer electrolyte that contains LiI, Hex₄NI and MPPII ternary iodides together with the DSC performance enhancer 4TBP.

2 Experimental

2.1 Materials

FTO transparent-conducting substrates with a sheet resistance of 10 Ω cm⁻² and ruthenium-based 535-bisTBA (N719) sensitizing dye were procured from Solaronix SA. TiO₂ Nanopowders, P25 (average particle size 21 nm), and P90 (average particle size 13 nm) were procured from Evonik, Germany. The starting materials, Hex₄NI, LiI, PEO (MW = 4,000,000), iodine (I₂), EC, PC, 1-methyl-3-propylimidazolium iodide, and 4-tert-butylpyridine (4TBP), with purity greater than 98%, were purchased from Aldrich. Prior to use, PEO, Hex₄NI, and LiI were vacuum dried for ~ 2 h at ~ 50 °C.

2.2 Preparation of multilayer TiO₂ photoanodes with 1–7 layers

For the preparation of the 1st layer of TiO₂ nano-particles in photoanodes, 0.5 g of TiO₂ nano-particles of the average size 13 nm (P90 powder) were grinded with 2 ml of 0.1 M HNO₃ for about 30 min in an agate mortar. To prevent coating of TiO₂ on the area of the FTO, which was needed for the electrical contacts, half of the FTO plate was masked by a piece of Scotch tape. Then, the TiO₂ slurry was spin-coated on a pre-cleaned FTO substrate (1 cm × 2 cm) at 2300 rpm for 2 min. Subsequently, this photoelectrode was air-dried under ambient conditions for 5 h, thereafter sintered in air at 450 °C for ~ 30 min. The same procedure was repeated for the preparation of the 2nd layer of TiO₂ photoanodes.

A TiO₂ dispersion is prepared by grinding 0.5 g of nano-particles of the size 21 nm (P25 powder) with 2 ml of 0.1 M HNO₃ in an agate mortar to coat the 3rd layer. The resulting slurry was spin coated at 1000 rpm for 2 min followed by sintering at 450 °C for 30 min. The 4th, 5th, 6th, and 7th layers were prepared by following the same spin coating and sintering processes that were used in the preparation of the 3rd layer. However, 0.1 g of polyethylene glycol (PEG (MW = 40,000)) and a few drops of Triton X 100 (surfactant) were added to the TiO₂ slurry used for the 4th, 5th, 6th, and 7th layers, mixed well before the spin coating process in order to reach a homogeneous mixture. The configuration of the multi-layered photoanode that contains 7 layers of TiO₂ nano-particles and prepared using the two different nano-particles sizes is illustrated in Fig. 1.

The series of photoanodes fabricated with 1 to 7 layers of TiO₂ nano-particles were immersed in a 0.3 mM

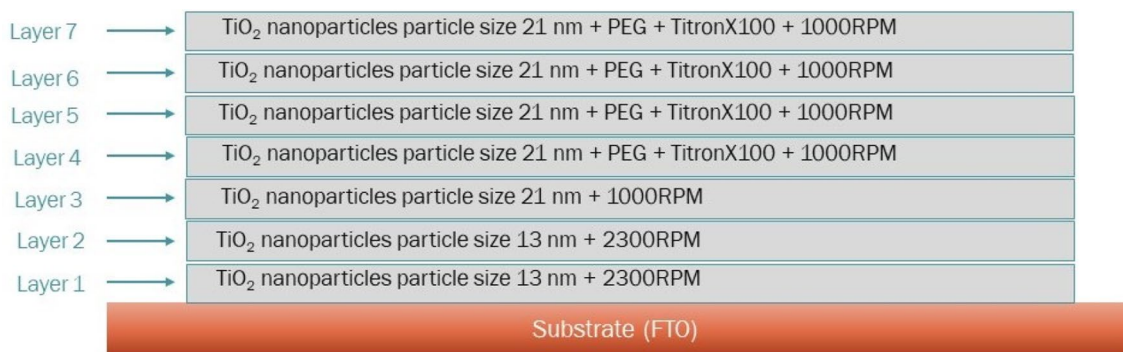


Fig. 1 A schematic diagram to illustrate the configuration of the multilayer photoelectrode with 7 layers of TiO₂ nano-particles

ethanol solution of N719 ruthenium dye for ~ 48 h. Prior to the immersion, the photoanodes were heated to ~ 100 °C, and the dye solution was heated to ~ 60 °C. The electrodes were washed gently with ethanol to remove the loosely bound dye after being taken out from the dye solution.

2.3 Preparation of gel polymer electrolyte

The gel polymer electrolyte was prepared according to the stoichiometric composition of $(EO)_{10}(EC)_{40}(PC)_{40}LiI_{(1.2)}(Hex_4Ni)_{(0.8)}(MPII)_{0.25}I_2_{(0.2)}$, where (EO) represents one monomer unit of PEO. The appropriate amount (0.85 mol) of performance enhancer (4TBP) relative to 10 mol of PEO was also added to the electrolyte. The amounts of MPII and 4TBP were decided based on our previous studies on performance enhancers [71, 72]. The LiI and Hex_4Ni binary salts composition was also selected from previously optimized systems in order to obtain DSCs with high performance [68, 73]. The solvent amount was decided from the preliminary studies done to get the gel nature for the electrolyte. For this purpose, a stock solution was prepared using EC:PC = 1:1 molar ratio, and a series of electrolytes was prepared by gradually increasing the solvent content and keeping the other components in the electrolyte fixed. Then, by using the inverted bottle test the optimum gel composition needed to obtain a non-flowing gel, electrolyte sample was selected. The molar ratios and weights of the components of the electrolyte are given in Table 1.

In a closed vial, corresponding amounts of Hex_4Ni , LiI, MPII, and 4TBP were dissolved in EC and PC co-solvents as the initial step of the electrolyte preparation. Next, a homogeneous mixture was obtained by a continuous stirring of the solution after adding the

appropriate amount of PEO. Then the mixture was heated to about 100 °C in constant stirring until it is converted to a transparent slurry. Then the mixture was allowed to cool down to ~ 40 °C, 12 mg of I_2 were added, and the mixing was continued for a few more minutes. The gel polymer electrolyte resulted from this process was characterized by ionic conductivity measurements and used for the solar cell fabrication.

2.4 Fabrication of the DSCs

A series of 7 different DSCs was assembled by sandwiching the gel polymer electrolyte between a Pt-sputtered counter-electrode and a dye-sensitized TiO_2 photoanode each with 1 to 7 spin-coated TiO_2 layers.

2.5 Characterization

2.5.1 Characterization of the layered TiO_2 photoanodes

The X-ray diffraction (XRD) technique was used for the structural characterization of 1–7-multilayer TiO_2 photoanodes. Cu K- α ($\lambda = 1.5405 \text{ \AA}$) radiation of the Rigaku Ultima IV X-Ray Diffractometer (KYOW-AGLAS-XATM, Japan) was used to produce the XRD patterns of the TiO_2 films.

Scanning electron microscopy (SEM) images of the TiO_2 layers were obtained using a Zeiss Evo LS15 SEM. These images were used to identify the morphology of the TiO_2 layers and also used to estimate the film thicknesses of the multilayer TiO_2 photoanodes.

The amount of dye adsorbed by each 1–7-layer TiO_2 photoanode was calculated with the help of their UV–visible absorption spectra. The reference graph for absorbance vs. concentration was plotted by measuring the absorbance for the known concentration of the dye solution. For this purpose, a known concentration of dye solution was prepared by dissolving 2 mg of ruthenium 535-bis TBA (N719 dye) in 0.1 mol dm^{-3} NaOH solution. Next, UV–visible absorption was measured by diluting the original solution. The graph of absorbance vs. concentration was plotted by measuring the peak absorption of the dye molecules at 500 nm. Subsequently, each dye-adsorbed photoanode was dipped in 3 ml of 0.1 mol dm^{-3} NaOH for 48 h to desorb the dye. The concentration of each dye-desorbed NaOH solution was determined using peak absorption at the 500 nm, and the reference graph (peak absorption data at the 500 nm against concentration) was calculated. Assuming that all the dye was

Table 1 Mass fractions and molar ratios of polymer, solvents, and performance enhancers used for the gel polymer electrolytes

Component	Weight/ mg	Molar ratio
PEO	100	10.0
EC	800	40.0
PC	927	40.0
MPII	15.1	0.25
Hex_4Ni	87.5	0.8
LiI	36.5	1.2
4TBP	26.1	0.85
I_2	11.5	0.2

desorbed into NaOH solution, the dye loading was calculated for each multilayer electrode.

2.5.2 Characterization of DSCs

Current–voltage (I – V) data were measured for about 3 h (at 10 min steps) for the fabricated solar cells with the light of 1000 W m^{-2} under continuous irradiation by using a PEC-LO1 solar simulator. The irradiated area of the DSC was 19 mm^2 . I – V data were measured using the potential scan rate 10 mV s^{-1} with the Pcell software and the Keithley 2400 source meter.

Electrochemical impedance spectroscopy (EIS) data of the solar cells were recorded by a Potentiostat (Autolab PGSTAT128N) frequency response analyzer (FRA) module. Impedance measurements were collected with NOVA 1.1 software. For the measurements, the cells were placed in a Faraday cage, and data were collected at room temperature in dark conditions. The measurements were conducted by applying a bias voltage similar to the V_{oc} of the respective cells, and the measurement frequency window was 0.1 Hz–1000 kHz.

3 Results and discussion

Altogether there are 7 layers in the photoelectrode studied in this work, and therefore, it is very difficult to investigate all the possible configurations ($7! = 5040$). Hence, the cell configuration was selected by using the following criteria.

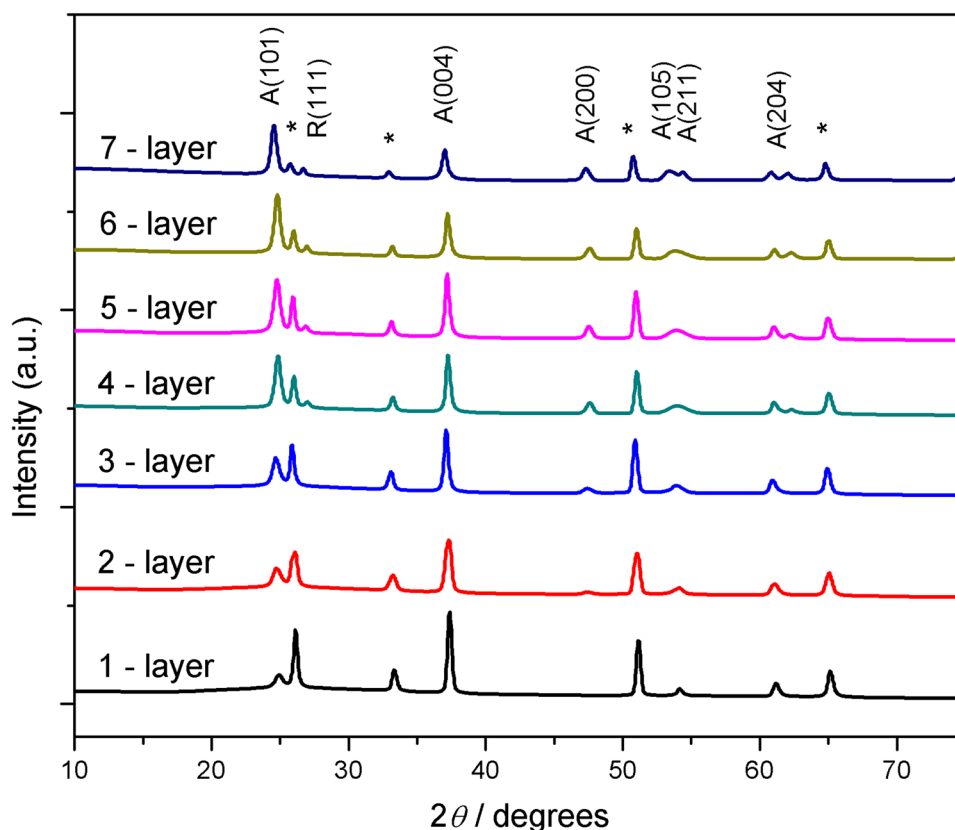
- (a) In general, when a photoelectrode is prepared for a DSSC, one or two dense or compact layers are used as the 1st layers (top layers) in order to get efficient charge transport (transport the injected electrons to TiO_2 from the excited dye toward the external circuit) and to prevent internal short circuit (to prevent leakage current between the electrolyte and FTO) [74–76]. These compact layers reduce the charge recombination [75]. Therefore, the pinhole-free and cracks-free layers are needed as 1st layers (top layers). In the present work, these top two layers were prepared using relatively higher RPM layers. In this way, we managed to prepare visually uniform and highly transparent compact top layers. Not only that small particle sizes used in the 1st layers are helpful to scatter the light to other porous layers and dye on them [77].
- (b) In addition, DSSC performance depends on dye adsorption which is governed by the effective surface area of the thicker TiO_2 on the compact layer. Therefore, in order to obtain a high porosity for these films, higher particle sizes (21 nm) were used. Further, it was observed that in these TiO_2 layers, the surface roughness is higher when the RPM is lower. Therefore, a lower RPM was used for the preparation of the thick TiO_2 layer. In addition, it was observed that when the particle size is higher (21 nm) and the RPM is lower, the films prepared are more translucent, indicating increased surface roughness and porosity.
- (c) PEG was added to the thick TiO_2 layers in order to improve the porosity of these layers. When electrodes were annealed at 450°C PEG gets decomposed and evaporate out. From XRD spectra, it is evident that no carbon residues remain in the sintered photoelectrode.
- (d) Triton X 100 (surfactant) is added to improve the porosity and to obtain a homogeneous distribution of the slurry on the substrate.
- (e) However, in the dense or compact layer preparation (for the top layers), PEG or Triton X 100 was not used as the purpose of these compact layers is different [78].

In addition to above-mentioned facts, prior knowledge from our previous DSC systems was used to select appropriate RPM, particle size, and inclusion of Triton X 100 and PEG.

3.1 XRD

XRD patterns of spin-coated TiO_2 photoanodes with 1–7 stacked layers prepared on FTO substrates are given in Fig. 2. The 2θ peak position values with their respective TiO_2 phases and relevant crystal planes are also shown in Fig. 2. Due to the clear diffraction peaks, it can be assumed that the TiO_2 phases present in the multilayer structure are well crystallized. The polycrystalline nature of the TiO_2 in the films is evident from the presence of several peaks in the XRD spectrum. Most of the peaks correspond to the anatase phase, except the peak that corresponds to the rutile (110) plane, at $2\theta = 27.4^\circ$, which indicates the TiO_2 films are predominantly in the anatase phase (JCPDS card no. 21–1276 and JCPDS 21–1272).

Fig. 2 XRD patterns of 1–7-layered spin-coated TiO₂ films



The peak at 27.4° is visible only when more than two layers are present in the sample, which can be due to the transformation of the anatase phase to the rutile phase because of the repeated thermal post-treatment [79–81]. According to the XRD pattern, there are peaks at 25.3° and 37.8°, which correspond to the (101) and (004) orientations of the anatase phase of TiO₂. Interestingly, it is observed that the intensity of the peak at 25.3° increases with the increasing number of layers, while the intensity of the peak at 37.8° decreases. The low intensity and peak broadening observed for the single- and double-layer films may be due to the smaller TiO₂ crystallite size of 13 nm (Fig. 1). The other XRD peaks located at 48.0°, 54.3°, 55.2°, 61.5°, and 65.5° belong to the orientations of the anatase phases indicated on the graphs.

3.2 SEM imaging

SEM images of the TiO₂ electrodes with 1, 2, 3, 4, 5, and 6 layers at 50,000 magnifications are shown in Fig. 3 – (a), (b), (c), (d), (e), and (f), respectively. The formation of crack-free mesoporous thin films with high porosity that offers high surface area is evident

from these SEM images. A large effective surface area in the TiO₂ photoanode is needed to improve the adsorption of the light-harvesting species, namely the N719 sensitizer dye used in this study. SEM images of the TiO₂ electrodes with 1, 2, 3, 4, 5, 6, and 7 layers are given in Figs. 4 – (a), (b), (c), (d), (e), (f), respectively, at 100,000 magnifications to understand the distribution size and the shapes of the crystallites and pores. The average crystallite size of the 1st and 2nd-layered electrodes agrees with the manufacturer's specification and is about 13 nm, while that of the 3–7 layers is about 21 nm. The compact nature of the 1st two layers is evident from the SEM images in Figs. 3(a), 3(b), and 4(a), 4(b). The presence of crack-free compact top layers is needed to overcome internal short circuiting (electrical contact between the electrolyte and FTO) and to get better electron transport from TiO₂ to FTO, while maintaining a low Ohmic resistance between the TiO₂ and the FTO layers. In addition, such compact layers scatter light in different directions, making light harvesting more efficient [77]. The higher porosity exhibited by 3- to 7-layered electrodes (Fig. 4) is important to achieve a higher effective surface area. High surface area enhances the dye adsorption, which

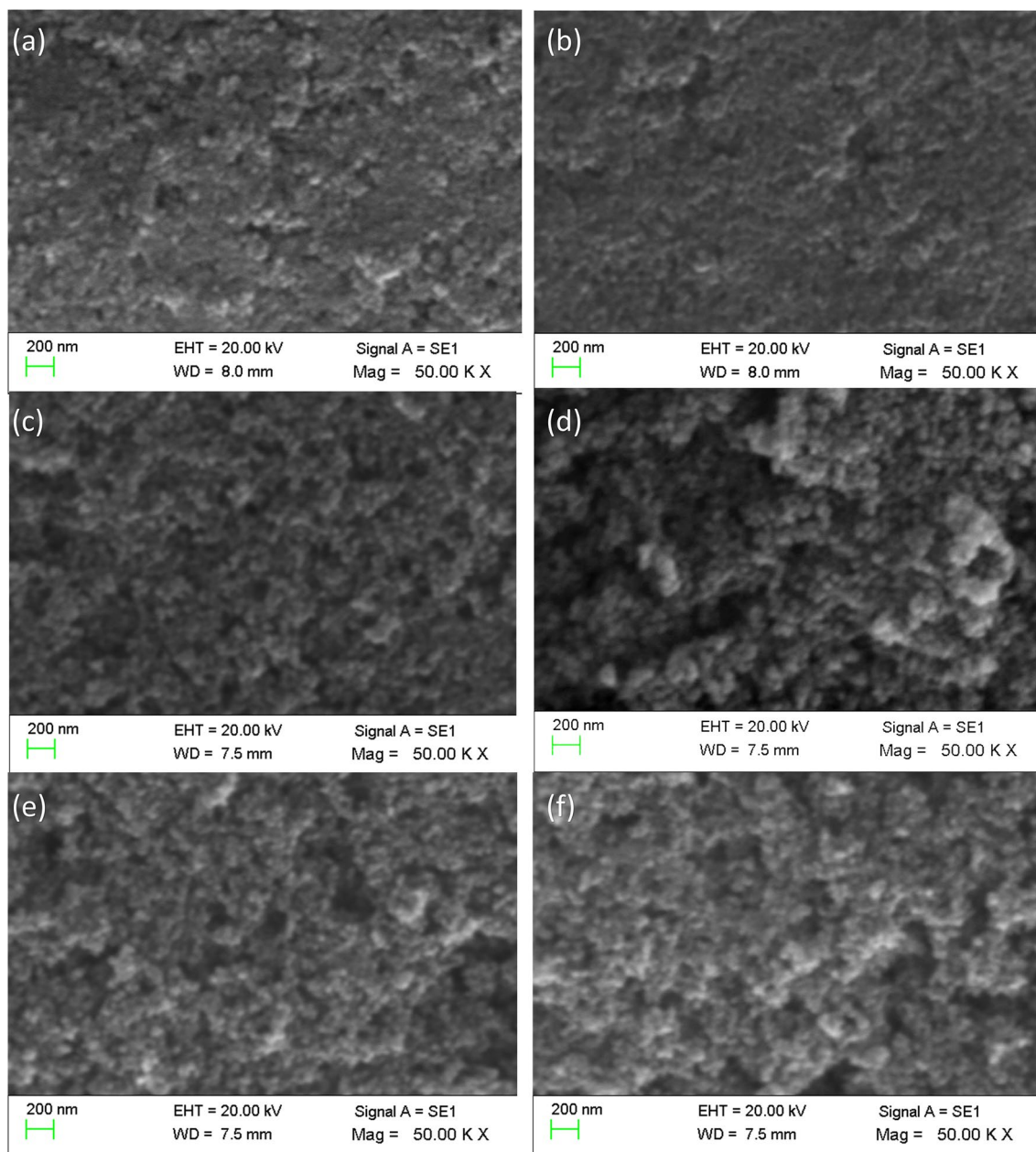


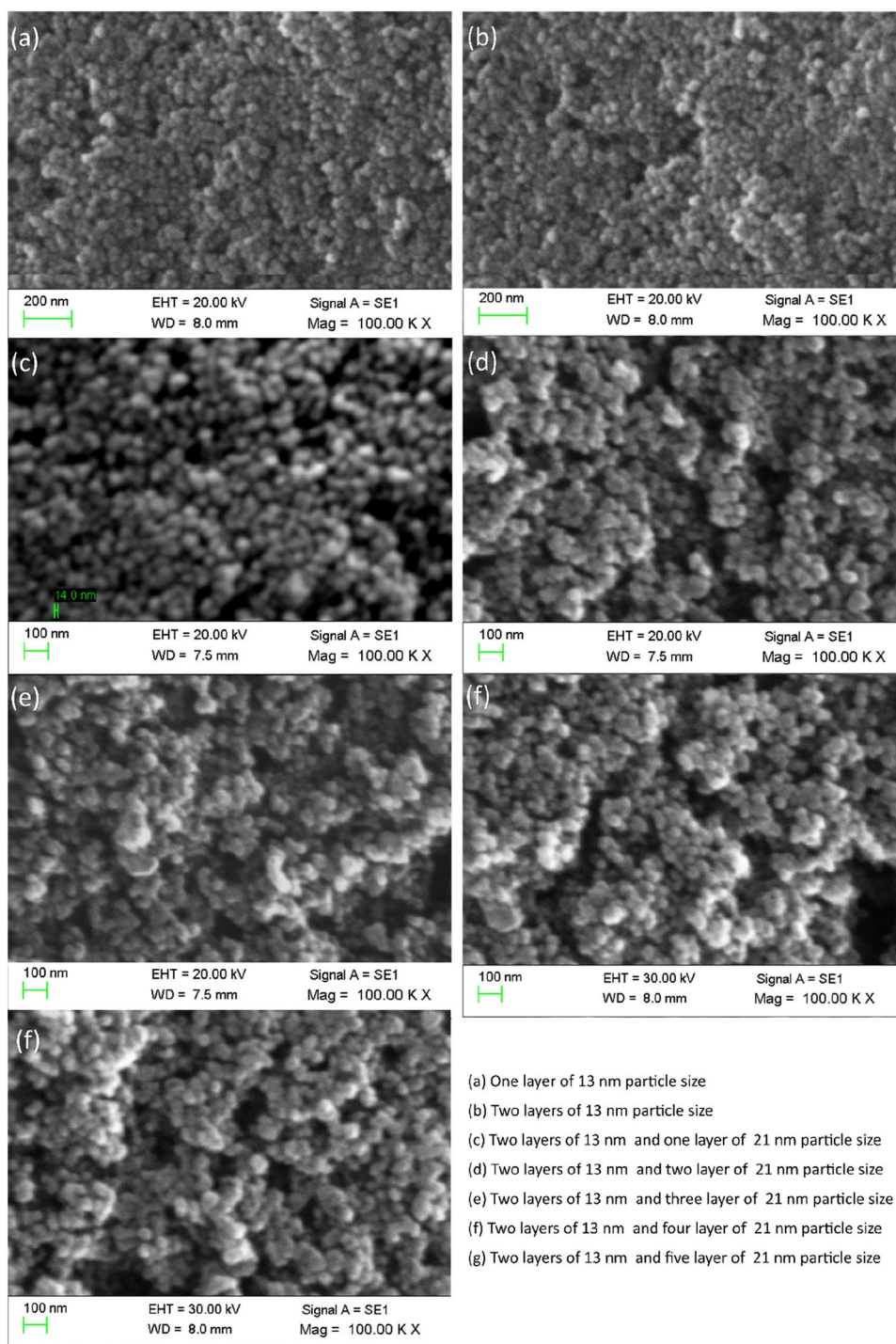
Fig. 3 SEM images of the TiO₂ films with 1, 2, 3, 4, 5, and 6 layers at 50,000 Magnification

improves the light-harvesting ability of the electrode. In addition, the rough surface morphology increases the electrode–electrolyte contact area reducing the interfacial charge transfer resistance, which finally helps achieve a higher photocurrent. For each layer, three SEM images were observed and all showed almost the same surface morphology confirming the high reproducibility of same morphology with this

method. The thickness of the sample could be reproduced within $\pm 6\%$ precision.

Transversal SEM images of 2, 3, 4, and 5-layered spin-coated TiO₂ films are shown in Fig. 5 (a), (b), (c), (d), respectively. The average thicknesses of the films prepared are given in Table 3. The thicknesses of the 1st and 2nd layers are almost the same ($\sim 0.5 \mu\text{m}$) and that of other layers is $\sim 1.0 \mu\text{m}$. The

Fig. 4 SEM images of the TiO₂ films with 1, 2, 3, 4, 5, 6, and 7 layers at 100,000 magnification



small layer thickness of the 1st and 2nd layers can be due to the use of small TiO₂ particle size (13 nm) and the layer thickness of the 3rd, 4th, and 5th layers

can be due to the use of relatively larger particle sizes (21 nm) during the film preparation.

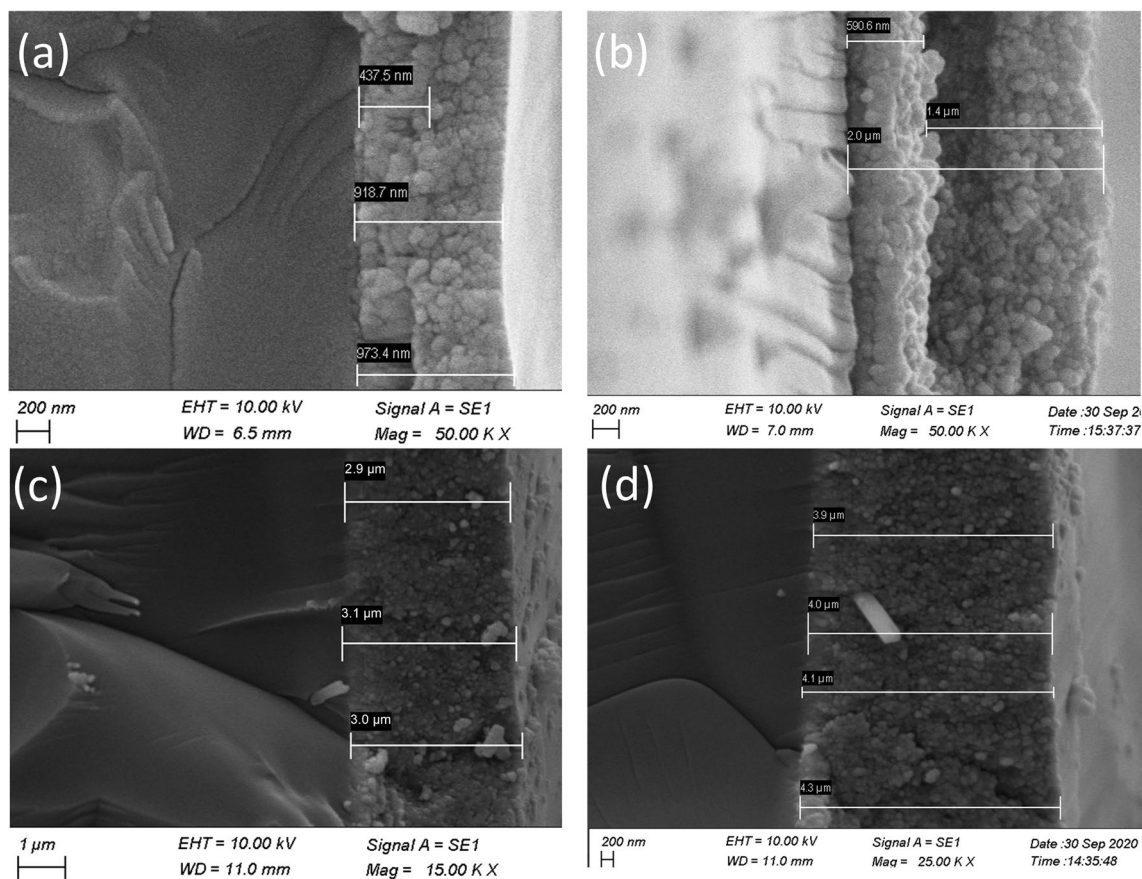


Fig. 5 Transversal SEM images of 2, 3, 4, and 5-layered spin-coated TiO_2 films are shown in **a**, **b**, **c**, and **d**, respectively

3.3 Dye adsorption

Since the photon-absorbing species in a DSC is the dye, the amount of the surface adsorption of the dye sensitizer is an important parameter in characterizing DSCs. In order to find surface dye concentration, at first UV–visible absorption spectra of known dye concentrations were investigated. The spectra of different dye concentrations of the solutions are given in Fig. 6 (a). It shows two absorption peaks, one at ~ 500 nm and the other at ~ 372 nm. Figure 6 (b) shows the graph of optical absorbance at 500 nm versus the concentration of the dye solution. According to the Beer–Lambert law, absorbance is directly proportional to the concentrations of the dissolved substance. Therefore, the calibration curve in Fig. 6 (b) was used to determine the concentrations of dye desorbed from the photoanodes.

The results were utilized to calculate the surface dye density (concentration) of each photoanode, which are given in Table 2. The calculated dye loading per

square centimeter of the TiO_2 film and absorbed dye weights are also provided in Table 2. As expected, the dye adsorption increases with the increasing number of spin-coated TiO_2 layers as well as the film thickness. For instance, the photoanode composed of 7-layered TiO_2 film exhibits the highest effective dye adsorption. One square centimeter of the 7-layer photoelectrode contains 7.50×10^{16} dye molecules ($124.5 \text{ nmol cm}^{-2}$), while the 1-layer photoelectrode contains 1.18×10^{16} molecules ($19.62 \text{ nmol cm}^{-2}$).

3.4 I–V and P–V characterization of DSCs

Current density versus cell potential (J – V) and power density versus cell potential (P – V) characteristic curves were used to determine the short-circuit current density (J_{SC}), the open-circuit voltage (V_{OC}), the fill factor (ff), and the energy conversion efficiency (η) of the DSCs fabricated in this work. Three cells were tested for each electrode composition, and all the cells exhibited almost similar results confirming the high

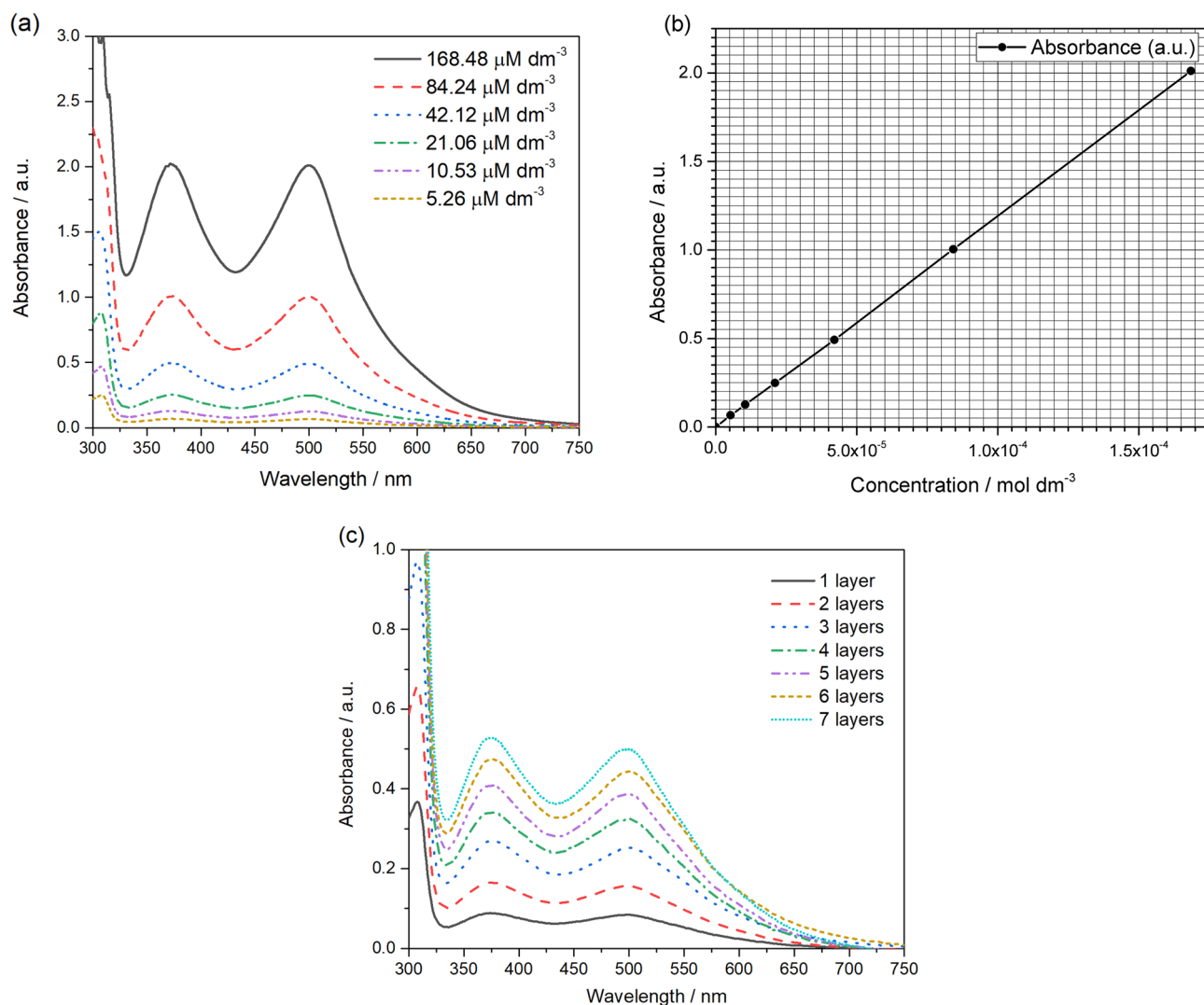


Fig. 6 **a** Absorbance vs wavelength for different concentrations of N719 dye solutions. **b** Absorbance vs concentration for N719 dye at 500 nm. **c** Absorbance vs wavelength for desorbed N719 dye from different photoanodes

Table 2 Amount of dye adsorbed with respect to the number of TiO_2 layers

Number of layers	Surface dye molar concentration (dye moles per unit area of the electrode) (nmol cm^{-2})	Surface dye concentration (number of molecules per unit area of the electrode) (10^{16} cm^{-2})	Surface dye density ($\mu\text{g cm}^{-2}$)
1	19.62	1.18	23.3
2	40.8	2.46	48.5
3	64.2	3.87	76.3
4	81.3	4.90	96.6
5	96.6	5.81	114.8
6	111.1	6.68	131.9
7	124.5	7.50	148.0

Table 3 Average values for J_{SC} , V_{OC} , ff , and η with respect to the number of TiO_2 layers

Layers	$J_{sc} / \text{mA cm}^{-2}$	V_{OC} / mV	$ff / \%$	$\eta / \%$
1	2.9 ± 0.06	820.0 ± 0.07	62 ± 3	1.5 ± 0.02
2	5.1 ± 0.52	751.2 ± 12.6	67 ± 3	2.5 ± 0.21
3	6.5 ± 0.71	753.6 ± 16.5	64 ± 2	3.1 ± 0.21
4	9.6 ± 0.54	724.0 ± 13.0	60 ± 2	4.2 ± 0.25
5	12.5 ± 0.26	698.0 ± 7.68	62 ± 2	5.5 ± 0.05
6	12.1 ± 0.31	708.8 ± 5.63	62 ± 2	5.3 ± 0.13
7	10.2 ± 0.45	706.1 ± 11.0	67 ± 2	4.9 ± 0.08

responsibility of results. Average values for J_{SC} , V_{OC} , ff , and η values of the DSCs are given in Table 3 with the number of TiO_2 layers in the photoanode. These average values were taken by continuously measuring J and V for 2 h at 10 min intervals. All the cells exhibited excellent stability during the 2 h measurement period. For example, plots of J_{SC} versus cell potential and power density versus cell potential are given in Fig. 7 as a function of irradiation time for the highest efficiency DSC containing 5-spin-coated TiO_2 layers.

In this study, V_{OC} exhibits a gradually decreasing trend with the increase of TiO_2 layers of the photoanode up to 5-layered TiO_2 film, and then it remains more or less unchanged (considering the error) or slightly increased with increasing thickness. The highest V_{OC} of 820.0 mV was shown by the DSC consisting of a single spin-coated TiO_2 layer, which exhibited the lowest efficiency and lowest J_{sc} . In DSSCs, several factors govern the open-circuit voltage due to the presence of a sensitized semiconductor layer and the electrolyte, counter-electrode, and several interfaces. The TiO_2 layer thickness plays a crucial role in determining the DSSCs performance. Typically, a thicker TiO_2 layer leads to a decrease in the open-circuit voltage (V_{oc}) of the cell as reported by several authors [82–87]. Simply the initial increase in charge carrier generation with improved dye adsorption along with increasing thickness might not be fully accompanied by an increase in charge carrier collection at the electrodes. This imbalance may lead to a decrease in the open-circuit voltage (V_{oc}) since V_{oc} is a measure of the electric potential difference between the electrodes when no current flows. However, the phenomenon can be understood considering several factors as explained below.

(a) Charge recombination effects: According to the light-harvesting mechanism of DSSCs after the

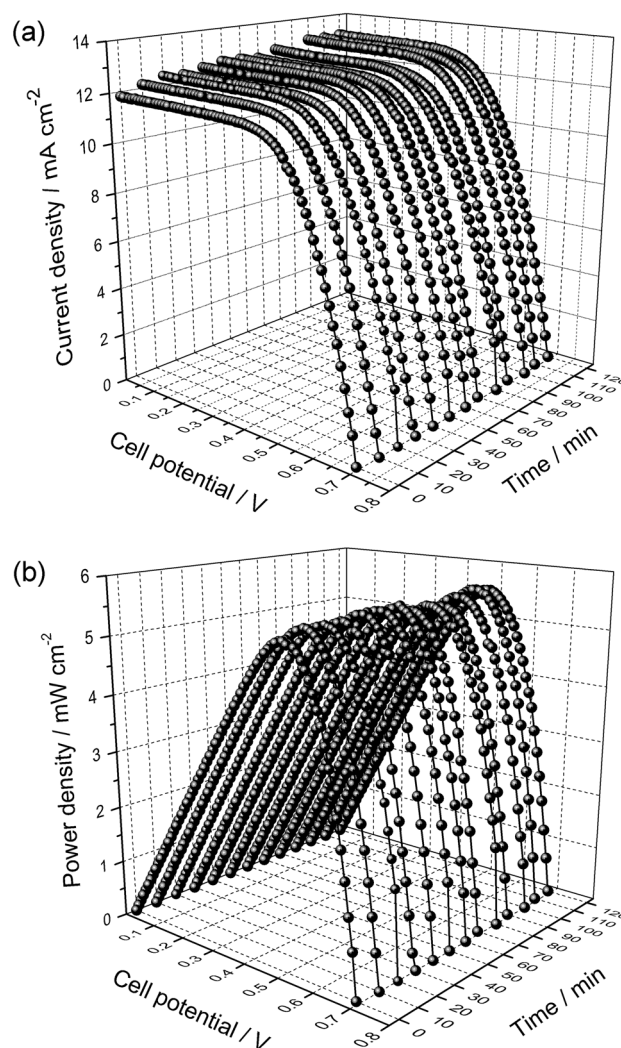


Fig. 7 **a** The photocurrent density versus potential (J – V) and **b** the power density versus cell potential (P – V) as a function of irradiation time of the DSC containing 5-spin-coated TiO_2 layers in the photoanode. Measurements were taken under steady irradiation of 1000 W m^{-2} (1.5 AM)

visible-light photons are absorbed by the dye molecules, they generate electron–hole pairs, or according to band theory, the conduction-band electrons and valence-band electrons. When the cells are connected to the external circuit, these photogenerated electrons are injected into the TiO_2 conduction band and then migrate through the TiO_2 layer to the FTO current collector, creating a photocurrent in the external circuit, while the holes remain in the dye. However, at the open-circuit condition, the external circuit is disconnected, and thus, there is no current through

the external circuit. In this situation, at the equilibrium, the rate of photogeneration is equal to the rate of recombination since there is no current through the external circuit. However, when the TiO₂ layer thickness is increased, the average distance that the electrons travel to reach the FTO current collector also increases. The increased transport path length that the electron should traverse to reach the current collector enhances the possibility of electron–hole recombination, reducing the net charge separation efficiency and, thus, lowering the Voc [82]. Further, due to the increase of the effective surface area with increasing thickness of the TiO₂ layer, which provides additional charge-recombination sites can drop the Voc [85, 88]. In addition, an increase in the number of trapping surface states, which improves the back electron transfer can also lower the Voc [82, 87]. In addition, Ito et al. [82] attributed this Voc drop also to the sharing of photoinjected conduction-band electrons by outer TiO₂ particle layers which lowers their quasi-Fermi level and hence the V_{OC}.

In order to understand the charge transport and transfer dynamics, electrochemical impedance spectroscopy of the DSSCs was analyzed. Using the impedance spectra, Bode phase diagrams were plotted (Fig. 8-(a)) to calculate the electron transport lifetimes

Table 4 Layer thickness of the photoanode (*L*) and electron transport lifetimes (τ_{tr}) and recombination lifetimes and diffusion length (D_L) of the DSSCs prepared by varying the number of TiO₂ layers in the photoanode

Layers	(<i>L</i>)/ μm	τ_{rec} / mS	τ_{tr} / mS	D_L / μm
1	0.5	13.19	0.25	2.73
2	1.0	15.92	0.21	4.02
3	2.0	30.32	0.14	5.23
4	3.0	32.15	0.19	8.12
5	4.3	46.67	0.60	13.65
6	5.2	39.99	1.00	13.35
7	6.2	28.94	0.25	11.47

(τ_{tr}) and recombination lifetimes (τ_{rec}) [85, 89, 90]. Figure 8(a) shows the Bode phase diagrams of the cell and the calculated parameters are given in Table 4.

(b) Diffusion length effects (D_L): The thickness of the TiO₂ film affects D_L (the distance of an electron can travel through a material before recombining with a hole) of the photogenerated electrons. In general, when the TiO₂ layer thickness increases, the D_L of electrons decreases since the possibility of recombination increases with the increasing thickness [91, 92]. In this study, electron diffusion lengths were calculated by using the following equation using analyzing impedance data [85, 93, 94]:

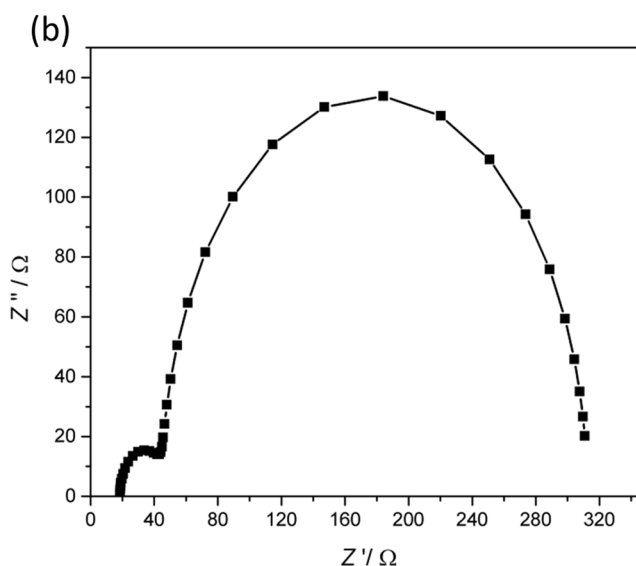
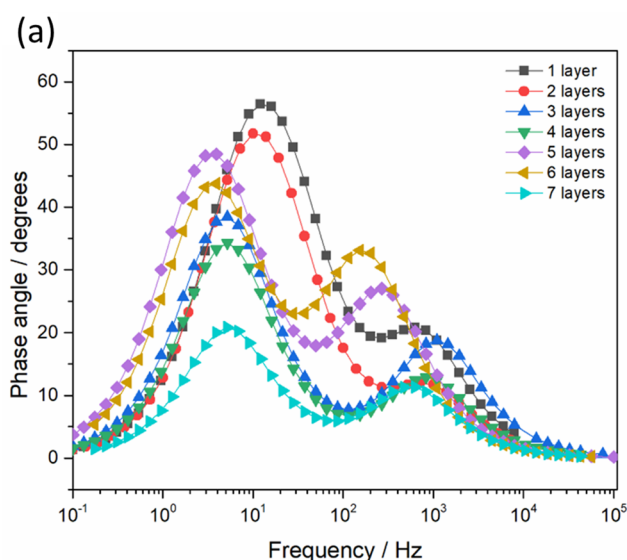


Fig. 8 **a** The Bode phase diagrams of the DSSCs prepared by varying the number of layers in the TiO₂ photoanode and **b** Nyquist plot of the DSSCs prepared DSS with 5-layer photoanode

$$D_L = L \sqrt{\frac{R_{rec}}{R_{tr}}}$$

where R_{rec} and R_{tr} are recombination resistance and charge transfer resistance. L is the sample thickness. Nyquist graphs were plotted to calculate R_{rec} and R_{tr} values. The Nyquist plot obtained for the 5-layer cell is given in Fig. 8(b). In Nyquist plots, the diameter of the high-frequency semicircle (on the left side) is attributed to the charge transport resistance R_{tr} while the diameter of the low-frequency semicircle (on the right side) (R_{rec}) is attributed to charge recombination. Sample thickness L was obtained by analyzing transverse SEM images. The calculated L and D_L values are given in Table 4.

Interestingly in this work, the calculated diffusion lengths increase up to five TiO_2 layers ($4.3 \mu\text{m}$) and then decrease with increasing number of layers. In addition, the calculated diffusion lengths are longer than the respective thinness of TiO_2 layers. Therefore, most of the electrons diffuse through the TiO_2 layers before recombination. However, the result in a shorter average diffusion length may have limited the effective transport of electrons to the electrode, resulting in a lower V_{oc} .

(c) Increased resistance effects: In a functional DSSC, photogenerated electrons (photocurrent) should travel to the FTO current collector through the TiO_2 layers. When the TiO_2 film thickness increases, the higher is the electrical resistance of the film since the resistance is directly proportional to the layer thickness. In addition, the inter-grain resistance of such nanocrystalline ceramic TiO_2 film from the increased number of grain boundaries, defects, and interfaces also contributes. This higher resistance can possibly impede the flow of electrons within the cell, leading to an internal electrical potential drop across the TiO_2 film. The result is reduced V_{oc} of the cell with increasing layer thickness. Therefore, the decreased V_{oc} with increasing layer thickness can very likely be due to the increased resistance of the sample with the increasing layer thickness. Considering the error of the V_{oc} values, it can be inferred that after 5 layers, the V_{oc} remains more or less constant or there can be a small V_{oc}

enhancement. In this region, the V_{oc} drop may be compensated by the enhanced carrier generation with increasing thickness and poor carrier collection due to enhanced resistance. Increased resistance can be understood due to the observed drop of J_{sc} in this region. In detail, the thicker layer can also enhance light absorption, allowing more photons to be absorbed and contribute to the generation of electron–hole pairs. This increased light absorption can partially compensate for the increased recombination, leading to a small improvement in V_{oc} .

(d) Rate of photoelectron generation. With the increasing layer thickness, the adsorbed surface dye concentration is increased, and therefore, the rate of photoelectron generation becomes higher for the thicker photoanodes. However, J_{sc} increase is exhibited only up to the 5th layer. When the TiO_2 layer thickness becomes higher (more than 5 layers), the observed photocurrent decrease could be due to the net effect of back electron transfer, resistive, and recombination losses. This can explain the V_{oc} values of the cells with 5, 6, and 7 layers (Table 3) which are slightly higher or unchanged. In principle, although the higher photoelectron generation is given by the cells with 7 layers, these cells exhibit lower photocurrent possibly due to the charge transport limitations of the cell as discussed above. In a functional cell, this mechanism would lead to higher charge generation but poor charge transport. The increased charge transport relaxation time of more-thicker sample may have influenced the slightly improved V_{oc} .

However, it should be noted that the relationship between TiO_2 layer thickness and V_{oc} is not a direct relationship. There is an indirect effect due to improved light absorption caused by enhanced dye absorption and improved electron injection. We can understand that in this case, the optimal thickness is given with the 5-layer film where the photocurrent and the efficiency are maximum. In this situation, the lowest V_{oc} is observed which can be a result of efficient charge transport dynamics which also increases the possibility of back electron transfer under open-circuit conditions. The increase of electron trapping surface states can also be a reason for V_{oc} drop [95]. At the optimum TiO_2 layer thickness above mentioned two competing processes balance to give the highest

overall cell performance. However, after the optimal thickness, for photoanodes with 6 and 7 layers, a small V_{oc} increase is observed which can be a result of increased resistances as inferred from the declined photocurrent.

The efficiency and the J_{SC} increased successively up to 5 layers of TiO_2 , then started to decrease (Table 3). Therefore, in these cells, the efficiency is clearly governed by the photocurrent. In general, the amount of light harvested by the dye molecules depends on the number of dye molecules dispersed on the photoelectrode, which governs the light-harvesting efficiency of the photoelectrode [96]. According to the dye adsorption data given in Table 2, the dye concentration in a photoanode gradually increases with the number of TiO_2 layers in the photoanode. Therefore, it can be concluded that the dye adsorption by the photoelectrode does not reach a saturation level with increasing thickness (or layers) up to 7 layers. However, the average values of efficiency and J_{SC} values increased with the increasing number of TiO_2 layers from 1 to 5 layers, as depicted in Table 3. The highest average efficiency of 5.5% and J_{SC} of 12.5 mA cm^{-2} are shown by the DSC containing 5 spin-coated TiO_2 layers. The thickness of this 5-layered TiO_2 film is $4 \text{ }\mu\text{m}$. It has also been reported that thicker photoanode films containing more TiO_2 P25 layers can adsorb more dye molecules than thinner films, leading to an increase in light-harvesting efficiency [97]. The 5-layer film prepared in this study contains 5.22×10^{16} dye molecules per square centimeter ($86.7 \text{ nmol cm}^{-2}$), which is much higher than that of the single-layered film, 1.18×10^{16} (Table 2). The increase in the efficiency and J_{SC} of DSCs with the increasing number of layers from 1 to 5 layers can, thus, be attributed to the increase in surface dye concentration (Tables 2 and 3).

Marandi et al. also observed an increase in efficiency with the increasing number of layers, which has also been attributed to the increase of dye adsorption [98]. As reported by these authors, the energy conversion efficiency in the DSC containing one transparent sub-layer of TiO_2 nanocrystals and two over-layers of TiO_2 P25 was 6.5% and the efficiency has increased to 7.2% for photoanodes made of two transparent sub-layers of TiO_2 nanocrystals with one P25 TiO_2 over-layer.

After exhibiting the peak efficiency and J_{SC} for the electrode with 5 TiO_2 layers, the efficiency and J_{SC} have decreased with further increase of the number of layers from 5 to 7 (Table 3). The DSC made of photoanodes with 4 and 6 TiO_2 layers showed an energy

conversion efficiency of 4.2 and 5.3% and J_{SC} of 9.6 and 12.1 mA cm^{-2} , respectively. The 5-layer film contains 5.22×10^{16} dye molecules per square centimeter ($86.7 \text{ nmol cm}^{-2}$), which is lower than the dye loading of 6- and 7-layer films (Table 2) [52]. There is a drop in efficiency and J_{SC} when the number of layers increases from 5 to 7. However, the efficiency and J_{SC} drops are not very considerable in the DSC consisting of 6-layer TiO_2 film and it showed penultimate efficiency and J_{SC} of 5.3% and 12.1 mA cm^{-2} , respectively. The drop of the J_{SC} and the efficiency of the cells that contain 6 and 7 TiO_2 layers are very likely to be due to the combined effect of 2 possible processes.

- (1) Diffusion lengths: The calculated diffusion lengths clearly follow the trend of J_{sc} . Therefore, the increased J_{sc} up to 5 layers and then observed decrease can be attributed to the variation of electron diffusion lengths given in Table 4. Although the sample thickness is higher, the average electron diffusion length J_{sc} variation has been affected by the variation of the diffusion length.
- (2) Recombination rates: Although longer electron transport paths can increase charge recombination (as mentioned), they can also provide more opportunities for electron-hole pair generation. If the recombination rate is relatively low (as evident by the shorter recombination time given in Table 4), the relatively longer path allows for more efficient electron recombination leading to a lower short-circuit current density.

As a result of all these effects, 6 and 7-layered cells show a lower photocurrent than that of 5-layer cells. This kind of decrease in the photocurrent and the efficiency with the increasing number of layers above a certain thickness have been observed in other studies too [85]. For example, an energy conversion efficiency of 7.2% was observed for the electrode containing one transparent sub-layer of TiO_2 nanocrystals with one over-layer of P25 but decreased to 6.7% for photoanodes made of two transparent sub-layers of TiO_2 nanocrystals with two P25 TiO_2 over-layers [98]. The authors relate the behavior to the effect of the increase in electron diffusion length in the TiO_2 layers with the increasing thickness of the photoanode.

J - V and P - V curves related to the highest efficiency for the DSCs composed of each photoelectrode are shown in Fig. 9. The highest J_{sc} and V_{oc} also showed the same behavior with the average values given in

Fig. 9 **a** The photocurrent density versus cell potential curves and **b** the power density versus cell potential curves that exhibited the highest efficiency for each dye-sensitized solar cells assembled with 1–7 layers of TiO₂. Measurements were taken under steady irradiation of 1000 W m⁻² (1.5 AM)

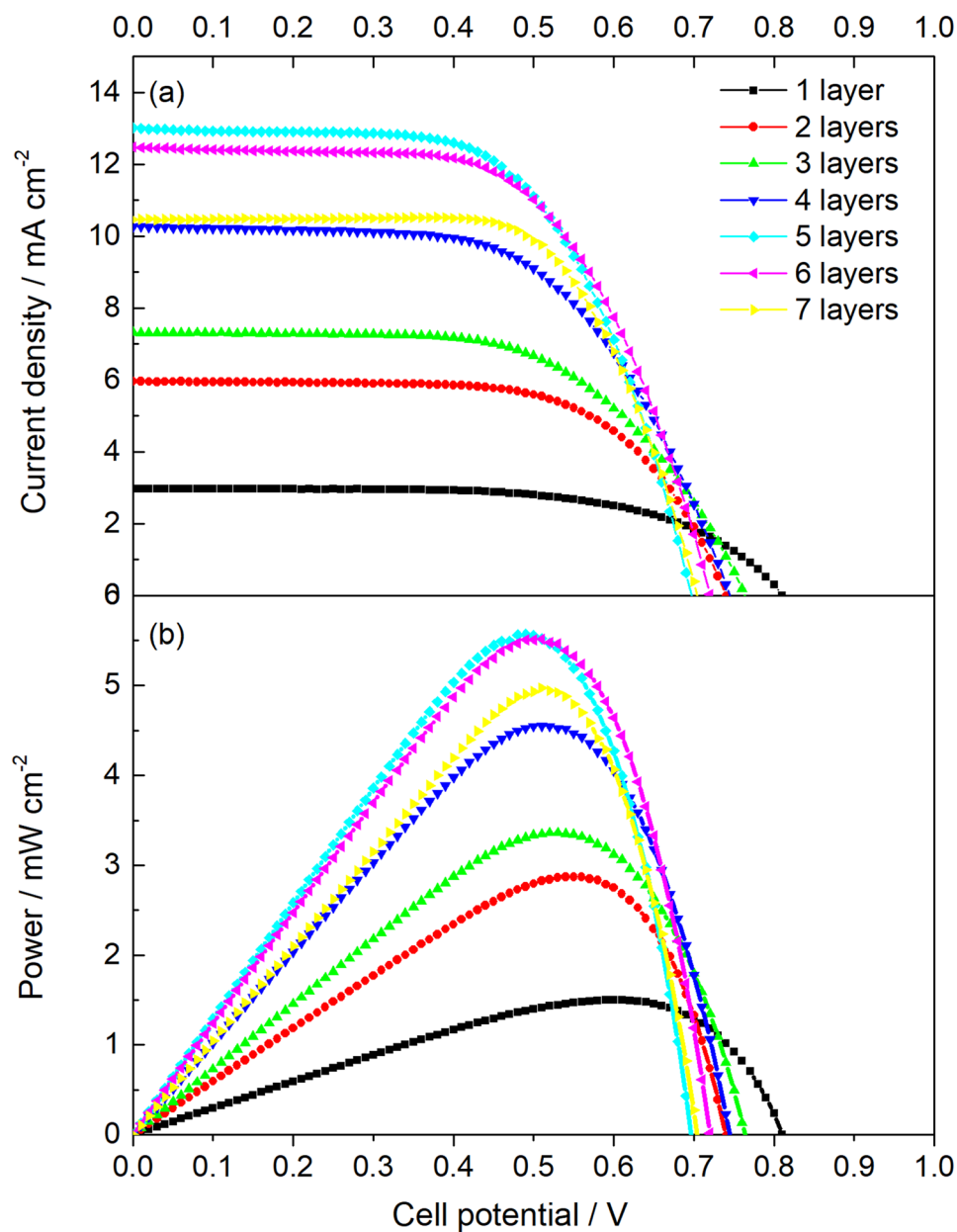


Table 5 Effective surface photoelectron generation rate, effective molecular photoelectron generation rate, and average time gap between two effective consecutive photon absorptions for the different photoanodes

Layers in the photoanode	1	2	3	4	5	6	7
Photoelectrons per second ($\times 10^{16} \text{ cm}^{-2} \text{ s}^{-1}$)	1.81	3.18	4.06	5.99	7.80	7.55	6.37
Surface dye concentration (nmole cm^{-2})	19.62	40.8	64.2	81.3	96.6	111.1	124.5
Effective molecular photoelectron generation rate (s^{-1})	1.53	1.29	1.05	1.22	1.34	1.13	0.85
Time gap between two effective consecutive photon absorptions (s)	0.65	0.77	0.95	0.82	0.74	0.88	1.18

Table 3. The highest J_{sc} , V_{oc} and efficiency values are 13 mA cm⁻², 0.7 V, and 5.56%, respectively. The highest J_{sc} values obtained from Fig. 9 (a) were used to calculate the photoelectrons generated per second from the unit area of the cell.

Since the J_{sc} values are known, the effective number of photoelectrons (photogenerated electrons that contribute to the current) generated per second from the unit area of each photoelectrode can be calculated using the following relationship.

$$\text{Photoelectrons per second per unit area} = \frac{J_{sc}}{e}$$

Therefore, since the surface dye density of each photoanode is known, the rate of effective photoelectron generation from a single dye molecule can be calculated from the following equation.

$$\text{Rate of effective photoelectron generation per dye molecule} = \frac{\text{Photoelectrons per second per unit area}}{\text{Surface dye concentration}}$$

The rates of effective surface photoelectron generation and effective molecular photoelectron generation and average time gap between two effective consecutive photon absorptions are given in Table 5 for the 7 different photoanodes. The rate of effective surface photoelectron generation follows the trend of J_{sc} variation. In general, the rate of effective photoelectron generation per dye molecule decreases with increasing layer thickness, which can be a result of the increase of idle dye molecules (due to the formation of dye aggregates and inefficient light scattering to the dye by TiO₂ layers) with increasing surface dye concentration (or number of layers). The fastest effective photoelectron generation (1.53 s⁻¹ molecule⁻¹) is exhibited by the single-layer photoelectrode, and the slowest (0.85 s⁻¹ molecule⁻¹) is shown by the 7-layer photoelectrode.

These results can be used to determine the average time gap (delay) between two effective consecutive effective photon absorptions, which is a highly important parameter to characterize a DSSC. The calculated delay times are given in Table 5 as a function of the number of layers in the photoanode. The general trend is that the average time gap increases with the increasing layer thickness, which can result from the increase in surface dye concentration. However, the photoanodes with 4 and 5 layers show relatively small delay time, which can be an effect of optimum dye distribution and light scattering of these photoelectrodes. The

rate of effective photoelectron generation and average time gap between two effective consecutive photon absorptions (s) are 1.34 molecule⁻¹ s⁻¹ and 0.74 s for the most efficient cell studied in this work.

4 Conclusion

This research was conducted to investigate the effect of thickness of a multilayer TiO₂ photoanode on the photocurrent and efficiency in a dye-sensitized solar cell. XRD results revealed the predominant presence of anatase phase of TiO₂ in all the layers of the photoanode electrode. The SEM images revealed that a single TiO₂ film is formed by merging all the layers in the 1 to 7-multi-layered TiO₂ photoanode and the thickness of the highest efficient DSC is about

$$\frac{\text{Photoelectrons per second per unit area}}{\text{Surface dye concentration}}$$

4.3 μm. The number of dye molecules adsorbed by each electrode gradually increased with the increasing thickness (number of layers) of the TiO₂ films. The J_{sc} and efficiency increase progressively as the number of TiO₂ layers increases up to 5 layers and then decreased for the photoanode with 6 or 7 layers. The 5-layer photoanode showed the maximum average efficiency of 5.5% and the maximum J_{sc} of 12.5 mA cm⁻². This electrode was found to contain 9.66 × 10⁻⁸ mol cm⁻² of adsorbed dye. All the DSCs composed of spin-coated 1 to 7- TiO₂-layered photoanodes exhibited excellent stability during the 2 h measurement period.

The present study introduces a way of determining the rate of effective photoelectron generation and average time gap between two effective consecutive photon absorptions. The rate of effective photoelectron generation and average time gap between two effective consecutive photon absorptions (s) are 1.34 molecule⁻¹ s⁻¹ and 0.74 s for the most efficient cell studied in this work.

Acknowledgements

The authors gratefully acknowledge the financial support from the Swedish Research Council, Sweden, grant number 2021-04889, as well as the support

received from the Postgraduate Institute of Science (PGIS), University of Peradeniya research grant (No. PGIS/2020/05).

Author contributions

All authors contributed to the conception, design, and analysis. The Material preparation, data collection, and the preparation first draft of the manuscript were done by T.M.W.J. Bandara, S.M.S. Gunathilake, and G.B.M.M.M. Nishshanke. All authors commented on previous versions of the manuscript and have read and approved the final manuscript. The project administration was done by I. Albinsson and T.M.W.J. Bandara.

Funding

Open access funding provided by University of Gothenburg. Financial support was received from the Swedish Research Council, Sweden, grant number 2021–04889, as well as from the Postgraduate Institute of Science (PGIS), University of Peradeniya research grant (No. PGIS/2020/05).

Data availability

The datasets generated and analyzed during the current study are available from the corresponding author on reasonable request.

Declarations

Competing interests The authors have no financial or non-financial interests to disclose.

Open Access This article is licensed under a Creative Commons Attribution 4.0 International License, which permits use, sharing, adaptation, distribution and reproduction in any medium or format, as long as you give appropriate credit to the original author(s) and the source, provide a link to the Creative Commons licence, and indicate if changes were made. The images or other third party material in this article are included in the article's Creative Commons licence, unless indicated otherwise in a credit line to

the material. If material is not included in the article's Creative Commons licence and your intended use is not permitted by statutory regulation or exceeds the permitted use, you will need to obtain permission directly from the copyright holder. To view a copy of this licence, visit <http://creativecommons.org/licenses/by/4.0/>.

References

1. B. O'Regan, M. Grätzel, A low-cost, high-efficiency solar cell based on dye-sensitized colloidal TiO₂ films. *Nature* **353**, 737–740 (1991)
2. A. Mahmood, Recent research progress on quasi-solid-state electrolytes for dye-sensitized solar cells. *J. Energy Chem.* **24**, 686–692 (2015)
3. F.O. Lenzmann, J.M. Kroon, Recent advances in dye sensitized solar cells. *Adv. OptoElectronics* (2007). <https://doi.org/10.1155/2007/65073>
4. K. Sharma, V. Sharma, S.S. Sharma, Dye-sensitized solar cells : fundamentals and current status. *Nanoscale Res. Lett.* **13**, 381 (2018). <https://doi.org/10.1186/s11671-018-2760-6>
5. J.-H. Yum, E. Baranoff, S. Wenger, M.K. Nazeeruddin, M. Grätzel, Panchromatic engineering for dye-sensitized solar cells. *Energy Environ. Sci.* **4**, 842 (2011)
6. N.T. Padmanabhan, H. John, Titanium dioxide based self-cleaning smart surfaces: A short review. *J. Environ. Chem. Eng.* **8**, 104211 (2020)
7. K. Song, Y. Cui, L. Liu, B. Chen, K. Hirose, M. Shahiduzzaman, S. Umez, Electro-spray deposited TiO₂ bilayer films and their recyclable photocatalytic self-cleaning strategy. *Sci. Rep.* **12**, 1–12 (2022)
8. T.T. Wei, F.F. Wang, X.Z. Li, J.H. Zhang, Y.R. Zhu, T.F. Yi, Towards high-performance battery systems by regulating morphology of TiO₂ materials. *Sustain. Mater. Technol.* **30**, 355 (2021)
9. W.J. Yu, W. He, C. Wang, F. Liu, L. Zhu, Q. Tian, H. Tong, X. Guo, Confinement of TiO₂ quantum dots in graphene nanoribbons for high-performance lithium and sodium ion batteries. *J. Alloy. Compd.* **898**, 162856 (2022)
10. Z. Li, S. Wang, J. Wu, W. Zhou, Recent progress in defective TiO₂ photocatalysts for energy and environmental applications. *Renew. Sustain. Energy Rev.* **156**, 111980 (2022)
11. K. Su, L. Li, S. Deng, Z. Gao, Q. Qin, J. Yang, J. Chen, Research progress of TiO₂ photocatalytic reduction of

- oxyanion pollutants in water: a mini review. *Green Chem. Lett. Rev.* **15**, 33–42 (2022)
12. M.R. Hoffmann, S.T. Martin, W. Choi, D.W. Bahnemann, Environmental applications of semiconductor photocatalysis. *Chem. Rev.* **95**, 69–96 (1995)
 13. J. Gong, K. Sumathy, Q. Qiao, Z. Zhou, Review on dye-sensitized solar cells (DSSCs): Advanced techniques and research trends. *Renew. Sustain. Energy Rev.* **68**, 234–246 (2017)
 14. A. Hagfeldt, G. Boschloo, L. Sun, L. Kloo, H. Pettersson, Dye-sensitized solar cells. *Chem. Rev.* **110**, 6595–6663 (2010)
 15. F.A. Grant, Properties of rutile (titanium dioxide). *Rev. Mod. Phys.* **31**, 646–674 (1959)
 16. L. Chu, J. Zhang, W. Liu, R. Zhang, J. Yang, R. Hu, X.A. Li, W. Huang, A facile and green approach to synthesize mesoporous anatase TiO₂ nanomaterials for efficient dye-sensitized and hole-conductor-free perovskite solar cells. *ACS Sustain. Chem. Eng.* **6**, 5588–5597 (2018)
 17. X. Chen, W. Dong, Y. Yao, L. Li, W. Hua, G. Zhuang, W. Song, Preparation of mesoporous anatase titania with large secondary mesopores and extraordinarily high photocatalytic performances. *Appl. Catal. B* **269**, 118756 (2020)
 18. L. Yang, W.W.-F. Leung, Application of a bilayer TiO₂ nanofiber photoanode for optimization of dye-sensitized solar cells. *Adv. Mater.* **23**, 4559–4562 (2011). <https://doi.org/10.1002/adma.201102717>
 19. R. Naphade M. Tathavadekar, J.P. Jog, S. Agarkar, S. Ogale, Plasmonic light harvesting of dye sensitized solar cells by Au-nanoparticle loaded TiO₂ nanofibers. *J. Mater. Chem. A* **2**, 975–984 (2014)
 20. W.Q. Wu, Y.F. Xu, C.Y. Su, D.B. Kuang, Ultra-long anatase TiO₂ nanowire arrays with multi-layered configuration on FTO glass for high-efficiency dye-sensitized solar cells. *Energy Environ. Sci.* **7**, 644–649 (2014)
 21. W.Q. Wu, B.X. Lei, H.S. Rao, Y.F. Xu, Y.F. Wang, C.Y. Su, D.B. Kuang, Hydrothermal Fabrication of Hierarchically Anatase TiO₂ Nanowire arrays on FTO Glass for Dye-sensitized Solar Cells. *Sci. Rep.* **3**, 1352 (2013)
 22. J. Liu, A. Wei, Z. Liu, F. Luo, Y. Zhao, Dye-sensitized solar cells based on multilayered ultrafine TiO₂ nanowire photoanodes. *J. Mater. Sci. Mater. Electron.* **25**, 4008–4011 (2014)
 23. H.Y. Chen, T.L. Zhang, J. Fan, D.B. Kuang, C.Y. Su, Electrospun hierarchical TiO₂ nanorods with high porosity for efficient dye-sensitized solar cells. *ACS Appl. Mater. Interfaces* **5**, 9205–9211 (2013)
 24. C.-J. Lin, W.-Y. Yu, S.-H. Chien, Rough conical-shaped TiO₂-nanotube arrays for flexible backilluminated dye-sensitized solar cells. *Appl. Phys. Lett.* (2008). <https://doi.org/10.1063/1.2992585>
 25. T.M.W.J. Bandara, W.J.M.J.S.R. Jayasundara, H.D.N.S. Fernando, M.A.K.L. Dissanayake, L.A.A. De Silva, I. Albinsson, M. Furlani, B.-E. Mellander, Efficiency of 10% for quasi-solid state dye-sensitized solar cells under low light irradiance. *J. Appl. Electrochem.* **45**, 289–298 (2015)
 26. C.P. Lee, P.W. Chen, C.T. Li, Y.J. Huang, S.R. Li, L.Y. Chang, P.Y. Chen, L.Y. Lin, R. Vittal, S.S. Sun, J.J. Lin, ZnO double layer film with a novel organic sensitizer as an efficient photoelectrode for dye-sensitized solar cells. *J. Power. Sources* **325**, 209–219 (2016)
 27. M.A.K.L. Dissanayake, H.K.D.W.M.N. Divarathna, C.B. Dissanayake, G.K.R. Senadeera, P.M.P.C. Ekanayake, C.A. Thotawattage, An innovative TiO₂ nanoparticle/nanofibre/nanoparticle, three layer composite photoanode for efficiency enhancement in dye-sensitized solar cells. *J. Photochem. Photobiol. A: Chem.* **322**, 110–118 (2016)
 28. M. Mojaddami, Z.A. Garmaroudi, M.R. Mohammadi, H.M. Hosseini, Efficient dye-sensitized solar cells based on TiO₂ nanoparticles and skein-like nanotubes: effect of arrangement modes of the layers and TiCl₄ treatment. *J. Taiwan Inst. Chem. Eng.* **61**, 138–146 (2016)
 29. G. Wang, W. Xiao, J. Yu, High-efficiency dye-sensitized solar cells based on electrospun TiO₂ multi-layered composite film photoanodes. *Energy* **86**, 196–203 (2015)
 30. M.S. Ahmad, A.K. Pandey, N. Abd Rahim, Advancements in the development of TiO₂ photoanodes and its fabrication methods for dye sensitized solar cell (DSSC) applications. A review. *Renew. Sustain. Energy Rev.* **77**, 89–108 (2017)
 31. U.A. Kamarulzaman, M.Y.A. Rahman, M.S. Su'ait, A.A. Umar, Effect of annealing treatment on multilayer TiO₂ films on the performance of dye-sensitized solar cells. *Optik* **218**, 164976 (2020)
 32. L. Wenqin, L. Hui, F. Wenpu, Y. Feng, W. Zihua, WO₃/TiO₂ composite multi-layer photoanode based dye sensitized solar cells: promoting electron injection process. *Optoelectron. Adv. Mater-Rapid Commun.* **15**, 271–277 (2021)
 33. A. Atli, A. Atilgan, A. Yildiz, Multi-layered TiO₂ photoanodes from different precursors of nanocrystals for dye-sensitized solar cells. *Sol. Energy* **173**, 752–758 (2018). <https://doi.org/10.1016/j.solener.2018.08.027>
 34. A. Roy, S. Bhandari, S. Sundaram, T.K. Mallick, Intriguing CeO₂-TiO₂ hybrid nanostructured photoanode resulting up to 46% efficiency enhancement for dye-sensitized solar cells. *Mater. Chem. Phys.* **272**, 125036 (2021)
 35. Z. Wang, H. Kawauchi, T. Kashima, H. Arakawa, Significant influence of TiO₂ photoelectrode morphology on the

- energy conversion efficiency of N719 dye-sensitized solar cell. *Coord. Chem. Rev.* **248**, 1381–1389 (2004)
36. M.N. Mustafa, S. Shafie, M.H. Wahid, Y. Sulaiman, Light scattering effect of polyvinyl- alcohol / titanium dioxide nanofibers in the dye-sensitized solar cell. *Sci. Rep.* **9**, 14952 (2019). <https://doi.org/10.1038/s41598-019-50292-z>
37. K. Cao, J. Lu, H. Li, Y. Shen, M. Wang, Efficient dye-sensitized solar cells using mesoporous submicrometer TiO₂ beads. *RSC Adv.* **5**, 62630–62637 (2015)
38. D. Erath, A. Filipović, M. Retzlaff, A.K. Goetz, F. Clement, D. Biro, R. Preu, Advanced screen printing technique for high definition front side metallization of crystalline silicon solar cells. *Sol. Energy Mater. Sol. Cells* **94**, 57–61 (2010)
39. S. Ito, P. Chen, P. Comte, M.K. Nazeeruddin, P. Liska, P. Pechy, M. Grätzel, Fabrication of screen-printing pastes from TiO₂ powders for dye-sensitized solar cells. *Prog. Photovoltaics Res. Appl.* **15**, 603–612 (2007)
40. H.H. Wang, C. Su, H.S. Chen, Y.C. Liu, Y.W. Hsu, N.M. Hsu, W.R. Li, Preparation of nanoporous TiO₂ electrodes for dye-sensitized solar cells. *J. Nanomater.* **2011**, 547103 (2011). <https://doi.org/10.1155/2011/547103>
41. F. Pichot, J.R. Pitts, B.A. Gregg, Low-temperature sintering of TiO₂ colloids: application to flexible dye-sensitized solar cells. *Langmuir* **16**, 5626–5630 (2000)
42. A. Chemseddine, K. Ullrich, T. Mete, F.F. Abdia, R. van de Krola, *J. Mater. Chem. A* **4**, 1723–1728 (2016)
43. L.A. DeSilva, M. Thakurdesai, T.M.W.J. Bandara, J. Preston, W. Johnson, A. Gaquere-Parker, S. Survase, Synthesis of dense TiO₂ nanoparticle multilayers using spin coating technique. *Appl. Phys. A* **124**, 314 (2018)
44. A.M. LaChance, Z. Hou, M.M. Farooqui, S.A. Carr, J.M. Serrano, C.E. Odendahl, M.E. Hurley, T.E. Morrison, J.L. Kubachka, N.T. Samuels, A.T. Barrett, Doctor-blade-assisted casting for forming thin composite coatings of montmorillonite and poly (vinyl alcohol). *Ind. Eng. Chem. Res.* **61**, 3766–3774 (2022)
45. Z. Wan, M. Xu, Z. Fu, D. Li, A. Mei, Y. Hu, Y. Rong, H. Han, Screen printing process control for coating high throughput titanium dioxide films toward printable mesoscopic perovskite solar cells. *Front. Optoelectron.* **12**, 344–351 (2019)
46. T.M.W.J. Bandara, L.A. DeSilva, K. Vignarooban, S.L.N. Senavirathna, R.L. Kulasiri, The voltammetric hysteresis behavior and potential scan rate dependence of a dye sensitized solar cells. *MRS Adv.* **4**, 865–871 (2019)
47. S. Sarker, H.W. Seo, Y.K. Jin, K.S. Lee, M. Lee, D.M. Kim, On the hysteresis of current density-voltage curves of dye-sensitized solar cells. *Electrochim. Acta* **182**, 493–499 (2015)
48. H. Yuan, W. Wang, D. Xu, Q. Xu, J. Xie, X. Chen, T. Zhang, C. Xiong, Y. He, Y. Zhang, Y. Liu, H. Shen, Outdoor testing and ageing of dye-sensitized solar cells for building integrated photovoltaics. *Sol. Energy* **165**, 233–239 (2018)
49. M.I. Asghar, K. Miettunen, J. Halme, P. Vahermaa, M. Toivola, K. Aitola, P. Lund, Review of stability for advanced dye solar cells. *Energy Environ. Sci.* **3**, 418–426 (2010)
50. K.J. Hwang, D.W. Park, S. Jin, S.O. Kang, D.W. Cho, Influence of dye-concentration on the light-scattering effect in dye-sensitized solar cell. *Mater. Chem. Phys.* **149**, 594–600 (2015)
51. E. Dell’Orto, L. Raimondo, A. Sassella, A. Abboto, Dye-sensitized solar cells: spectroscopic evaluation of dye loading on TiO₂. *J. Mater. Chem.* **22**, 11364–11369 (2012)
52. T.M.W.J. Bandara, L.A. DeSilva, J.L. Ratnasekera, K.H. Hettiarachchi, A.P. Wijerathna, M. Thakurdesai, J. Preston, I. Albinsson, B.-E. Mellander, High efficiency dye-sensitized solar cell based on a novel gel polymer electrolyte containing RbI and tetrahexylammonium iodide (Hex₄NI) salts and multi-layered photoelectrodes of TiO₂ nanoparticles. *Renew. Sustain. Energy Rev.* **103**, 282–290 (2019)
53. R.S. Shelke, S.B. Thombre, S.R. Patrikar, Status and perspectives of dyes used in dye sensitized solar cells. *Int. J. Renew. Energy Resour.* **3**, 54–61 (2017)
54. F. Bella, J. Popovic, A. Lamberti, E. Tresso, C. Gerbaldi, J. Maier, Interfacial effects in solid-liquid electrolytes for improved stability and performance of dye-sensitized solar cells. *ACS Appl. Mater. Interfaces* **9**, 37797–37803 (2017)
55. L.P. Teo, M.H. Buraidah, A.K. Arof, Polyacrylonitrile-based gel polymer electrolytes for dye-sensitized solar cells: a review. *Ionic* **26**, 4215–4238 (2020)
56. O.A. Ieperuma, Gel polymer electrolytes for dye sensitised solar cells: a review. *Mater. Technol.* **28**, 65–70 (2013)
57. N. Jiang, T. Sumitomo, T. Lee, A. Pellaroque, O. Bellon, D. Milliken, H. Desilvestro, High temperature stability of dye solar cells. *Sol. Energy Mater. Sol. Cells* **119**, 36–50 (2013)
58. J. Wen, Z. Sun, Y. Qiao, Y. Zhou, Y. Liu, Q. Zhang, Y. Liu, S. Jiao, Ti₃C₂ MXene-reduced graphene oxide composite polymer-based printable electrolyte for quasi-solid-state dye-sensitized solar cells. *ACS Appl. Energy Mater.* **5**, 3329–3338 (2022)
59. V. Subramanian, K.H. Prasad, H.T. Das, K. Ganapathy, S. Nallani, T. Maiyalagan, Novel dispersion of 1D nanofiber fillers for fast ion-conducting nanocomposite polymer blend quasi-solid electrolytes for dye-sensitized solar cells. *ACS Omega* **7**, 1658–1670 (2022)

60. M. Gerosa, A. Sacco, A. Scalia, F. Bella, A. Chiodoni, M. Quaglio, E. Tresso, S. Bianco, Toward totally flexible dye-sensitized solar cells based on titanium grids and polymeric electrolyte. *IEEE J. Photovoltaics* **6**, 498–505 (2016)
61. F. Bella, A. Verna, C. Gerbaldi, Patterning dye-sensitized solar cell photoanodes through a polymeric approach: A perspective. *Mater. Sci. Semicond. Process.* **73**, 92–98 (2018)
62. F. Bella, A. Lamberti, S. Bianco, E. Tresso, C. Gerbaldi, C.F. Pirri, Floating, flexible polymeric dye-sensitized solar-cell architecture: the way of near-future photovoltaics. *Adv. Mater. Technol.* (2016). <https://doi.org/10.1002/admt.201600002>
63. S. Mozaffari, M.R. Nateghi, M. Borhanizarandi, Effects of water-based gel electrolyte on the charge recombination and performance of dye-sensitized solar cells. *J. Solid State Electrochem.* **18**, 2589–2598 (2014)
64. F. Bella, L. Porcarelli, D. Mantione, C. Gerbaldi, C. Barolo, M. Grätzel, D. Mecerreyes, A water-based and metal-free dye solar cell exceeding 7% efficiency using a cationic poly(3, 4-ethylenedioxythiophene) derivative. *Chem. Sci.* **11**, 1485–1493 (2020)
65. N. Pavithr, A.M. Asiri, S. Anandan, Fabrication of dye sensitized solar cell using gel polymer electrolytes consisting poly(ethylene oxide)-acetamide composite. *J. Power. Sources* **286**, 346–353 (2015)
66. T.M.W.J. Bandara, M.A.K.L. Dissanayake, W.J.M.J.S.R. Jayasundara, I. Albinsson, B.-E. Mellander, Efficiency enhancement in dye sensitized solar cells using gel polymer electrolytes based on a tetrahexylammonium iodide and MgI_2 binary iodide system. *Phys. Chem. Chem. Phys.* **14**, 8620–8627 (2012)
67. C.K. Ling, M.M. Aung, L.C. Abdullah, L.H. Ngee, H. Uyama, A short review of iodide salt usage and properties in dye sensitized solar cell application: Single vs binary salt system. *Sol. Energy* **206**, 1033–1038 (2020)
68. G.B.M.M.M. Nishshanke, A.K. Arof, T.M.W.J. Bandara, Review on mixed cation effect in gel polymer electrolytes for quasi solid-state dye-sensitized solar cells. *Ionics* **26**, 3685–3704 (2020)
69. C.Y. Tan, N.M. Saidi, N.K. Farhana, F.S. Omar, M.M. Algaradah, S. Bashir, S. Ramesh, K. Ramesh, Improved ionic conductivity and efficiency of dye-sensitized solar cells with the incorporation of 1-methyl-3-propylimidazolium iodide. *Ionics* **26**, 3173–3183 (2020)
70. G. Schlichthor, S.Y. Huang, J. Sprague, A.J. Frank, Band edge movement and recombination kinetics in dye-sensitized nanocrystalline TiO_2 solar cells: a study by intensity modulated photovoltage spectroscopy. *J. Phys. Chem. B* **101**, 8141–8155 (1997)
71. T.M.W.J. Bandara, H.D.N.S. Fernando, M. Furlani, I. Albinsson, J.L. Ratnasekera, L.A. DeSilva, M.A.K.L. Dissanayake, B.-E. Mellander, Combined effect of alkaline cations and organic additives for iodide ion conducting gel polymer electrolytes to enhance efficiency in dye sensitized solar cells. *Electrochim. Acta* **252**, 208–214 (2017)
72. T.M.W.J. Bandara, H.D.N.S. Fernando, M. Furlani, I. Albinsson, M.A.K.L. Dissanayake, B.-E. Mellander, Performance enhancers for gel polymer electrolytes based on LiI and RbI for quasi-solid-state dye sensitized solar cells. *RSC Adv.* **6**, 103683–103691 (2016)
73. T.M.W.J. Bandara, W.J.M.J.S.R. Jayasundara, M.A.K.L. Dissanayake, H.D.N.S. Fernando, M. Furlani, I. Albinsson, B.-E. Mellander, Quasi solid state polymer electrolyte with binary iodide salts for photo-electrochemical solar cells. *Int. J. Hydrogen Energy* **39**, 2997–3004 (2014)
74. M.N. Mustafa, S. Shafie, M.H. Wahid, Y. Sulaiman, Preparation of TiO_2 compact layer by heat treatment of electrospun TiO_2 composite for dye-sensitized solar cells. *Thin Solid Films* **693**, 137699 (2020)
75. K. Nonomura, N. Vlachopoulos, E. Unger, L. Häggman, A. Hagfeldt, G. Boschloo, Blocking the charge recombination with diiodide radicals by TiO_2 compact layer in dye-sensitized solar cells. *J. Electrochem. Soc.* **166**, B3203 (2019)
76. M.A.K.L. Dissanayake, T. Jaseetharan, G.K.R. Senadeera, J.M.K.W. Kumari, C.A. Thotawatthage, B.-E. Mellander, I. Albinsson, M. Furlani, Highly efficient, PbS: Hg quantum dot-sensitized, plasmonic solar cells with TiO_2 triple-layer photoanode. *J. Solid State Electrochem.* **23**, 1787–1794 (2019)
77. M.N. Mustafa, Y. Sulaiman, Review on the effect of compact layers and light scattering layers on the enhancement of dye-sensitized solar cells. *Sol. Energy* **215**, 26–43 (2021)
78. A.I. Maldonado-Valdivia, E.G. Galindo, M.J. Ariza, M.J. Garcia-Salinas, Surfactant influence in the performance of titanium dioxide photoelectrodes for dye-sensitized solar cells. *Sol. Energy* **91**, 263–272 (2013)
79. H. Mehranpour, M. Askari, M.S. Ghamsari, H. Farzalibeik, Study on the phase transformation kinetics of sol-gel driven nanoparticles. *J. Nanomater.* (2010). <https://doi.org/10.1155/2010/626978>
80. H. Uchida, M. N., Patel, R. A., May, G. Gupta, K. J. Stevenson, K. P. Johnston, Highly-ordered mesoporous titania thin films prepared via surfactant assembly on conductive indium-tin-oxide/glass substrate and its optical properties. *Thin Solid Films* **518**, 3169–3176 (2010)
81. P. Innocenzi, L. Malfatti, T. Kidchob, S. Enzo, G.D. Ventura, U. Schade, A. Marcelli, Correlative analysis of the

- crystallization of sol–gel dense and mesoporous anatase titania films. *J. Phys. Chem. C* **114**, 22385–22391 (2010)
82. S. Ito, S.M. Zakeeruddin, R. Humphry-Baker, P. Liska, R. Charvet, P. Comte, M.K. Nazeeruddin, P. Péchy, M. Takata, H. Miura, S. Uchida, High-efficiency organic-dye-sensitized solar cells controlled by nanocrystalline-TiO₂ electrode thickness. *Adv. Mater.* **18**, 1202–1205 (2006)
 83. M. Fitra, I. Daut, M. Irwanto, N. Gomesh, Y.M. Irwan, Effect of TiO₂ thickness dye solar cell on charge generation. *Energy Procedia* **36**, 278–286 (2013)
 84. D.G. Lee, M.C. Kim, B.J. Kim, D.H. Kim, S.M. Lee, M. Choi, H.S. Jung, Effect of TiO₂ particle size and layer thickness on mesoscopic perovskite solar cells. *Appl. Surf. Sci.* **477**, 131–136 (2019)
 85. J.M.K.W. Kumari, N. Sanjeevadarshini, M.A.K.L. Dissanayake, G.K.R. Senadeera, C.A. Thotawatthage, The effect of TiO₂ photo anode film thickness on photovoltaic properties of dye-sensitized solar cells. *Ceylon J. Sci.* **45**, 33–41 (2016)
 86. E. Supriyanto, N. Alviati, H.A. Kartikasari, L. Rohman, K. Triyana. Simulation of electron diffusion coefficient interpretation on the optimum thickness of TiO₂ photoanode in dye-sensitized solar cell (DSSC). In *IOP conference series: materials science and engineering*, Vol. 515 (2019, April) No. 1, p. 012058. IOP Publishing.
 87. M.G. Kang, K.S. Ryu, S.H. Chang, N.G. Park, J.S. Hong, K.J. Kim, Dependence of TiO₂ film thickness on photocurrent-voltage characteristics of dye-sensitized solar cells. *Notes* **25**, 743 (2004)
 88. S. Kambe, S. Nakade, Y. Wada, T. Kitamura, S. Yanagida, Effects of crystal structure, size, shape and surface structural differences on photo-induced electron transport in TiO₂ mesoporous electrodes. *J. Mater. Chem.* **12**, 723–728 (2002)
 89. J.H. Yun, A.J. Mozer, P. Wagner, D.L. Offier, R. Amal, Y.H. Ng, Light soaking effect driven in porphyrin dye-sensitized solar cells using 1D TiO₂ nanotube photoanodes. *Sustain. Mater. Technol.* **24**, e00165 (2020)
 90. S. Sarker, A.J. Ahammad, H.W. Seo, D.M. Kim, Electrochemical impedance spectra of dye-sensitized solar cells: fundamentals and spreadsheet calculation. *Int. J. Photoenergy* **2014**, 1–17 (2014)
 91. D. Kumar, K.P.S. Parmar, P. Kuchhal, Analysis of charge transport properties of dye-sensitized solar cell (DSSC) with TiO₂ working electrode by employing electrochemical impedance spectroscopy (EIS) network. *Int. J. Renew. Energy.* **19**, 22–26 (2021)
 92. V. Baglio, M. Girolamo, V. Antonucci, A.S. Aricò, Influence of TiO₂ film thickness on the electrochemical behaviour of dye-sensitized solar cells. *Int. J. Electrochem. Sci.* **6**, 3375–3384 (2011)
 93. J. Bisquert, I. Mora-Seró, Simulation of steady-state characteristics of dye-sensitized solar cells and the interpretation of the diffusion length. *J. Phys. Chem. Lett.* **1**, 450–456 (2010)
 94. J. Bisquert, F. Fabregat-Santiago, I. Mora-Sero, G. Garcia-Belmonte, S. Gimenez, Electron lifetime in dye-sensitized solar cells: theory and interpretation of measurements. *The Journal of Physical Chemistry C* **113**, 17278–17290 (2009)
 95. S. Kambe, S. Nakade, Y. Wada, T. Kitamura, S. Yanagida, Effects of crystal structure, size, shape and surface structural differences on photo-induced electron transport in TiO₂ mesoporous electrodes. *J. Mater. Chem.* **12**, 723–728 (2002)
 96. D.N. Joshi, S. Sudhakar, R.V. Nair, R. Arun Prasath, Swift sol-gel synthesis of mesoporous anatase-rich TiO₂ aggregates via microwave and a lyophilization approach for improved light scattering in DSSCs. *J. Mater. Sci.* **52**, 2308–2318 (2017)
 97. M. Hamadian, A. Gravand, M. Farangi, V. Jabbari, The Effect of the Thickness of Nanoporous TiO₂ Film on the Performance of Nanocrystalline Dye-Sensitized Solar Cell. *Proceeding of the 5th symposium on advances in science and technology*, Mashad, Iran 2011.
 98. M. Marandi, S. Sabet, M. Naeimi, F. Ahmadloo, Fabrication of dye-sensitized solar cells with multilayer photoanodes of hydrothermally grown TiO₂ nanocrystals and P25 TiO₂ nanoparticles. *Bull. Mater. Sci.* **39**, 1403–1410 (2016). <https://doi.org/10.1007/s12034-016-1289-5>

Publisher's Note Springer Nature remains neutral with regard to jurisdictional claims in published maps and institutional affiliations.